Visualizing Molecular Polar Order in Tissues via Electromechanical Coupling

Denise Denning[a,b], Sofiane Alilat[a,*], Stefan Habelitz[c], Andrzej Fertala[d], and Brian J. Rodriguez[a,b,†]

[a] *Conway Institute of Biomolecular and Biomedical Research, University College Dublin, Belfield, Dublin 4, Ireland.*

[b] *School of Physics, University College Dublin, Belfield, Dublin 4, Ireland.*

[c] *Department of Preventive and Restorative Dental Sciences, University of California, 707 Parnassus Avenue, San Francisco, CA 94143-0758, USA.*

[d] *Department of Orthopaedic Surgery, Thomas Jefferson University, 1015 Walnut Street, Philadelphia, PA 19107, USA.*

Corresponding author:
Dr. Brian J. Rodriguez
Tel: +353-1-716-6744
Fax: +353-1-716-6701
Email: brian.rodriguez@ucd.ie
Address:
Conway Institute of Biomolecular and Biomedical Research,
University College Dublin,
Belfield,
Dublin 4,
Ireland.

---

[*] Currently at ST Microelectronics

[†] Corresponding author: brian.rodriguez@ucd.ie

Electron microscopy (EM) and atomic force microscopy (AFM) techniques have long been used to characterize collagen fibril ordering and alignment in connective tissues. These techniques, however, are unable to map collagen fibril polarity, *i.e*., the polar orientation that is directed from the amine to the carboxyl termini. Using a voltage modulated AFM-based technique called piezoresponse force microscopy (PFM), we show it is possible to visualize both the alignment of collagen fibrils within a tissue and the polar orientation of the fibrils with minimal sample preparation. We demonstrate the technique on rat tail tendon and porcine eye tissues in ambient conditions. In each sample, fibrils are arranged into domains whereby neighbouring domains exhibit opposite polarizations, which in some cases extend to the individual fibrillar level. Uniform polarity has not been observed in any of the tissues studied. Evidence of anti-parallel ordering of the amine to carboxyl polarity in bundles of fibrils or in individual fibrils is found in all tissues, which has relevance for understanding mechanical and biofunctional properties and the formation of connective tissues. The technique can be applied to any biological material containing piezoelectric biopolymers or polysaccharides.

Keywords: atomic force microscopy, piezoresponse force microscopy, collagen, piezoelectricity, polar ordering, eye tissues, tendon.

1. Introduction

Properties of biological materials depend strongly on structure, cross-links, and gradients (Dunlop and Fratzl, 2010). These materials generally contain hierarchically-structured mineral and protein or polysaccharide phases, which combine to yield a material tougher than either constituent part alone (Buehler, 2006; Ji and Gao, 2004). In bone, the hardness and fracture strength exhibited on multiple length scales is due to the configuration of nanoscale crystals of a hard, mineral phase, hydroxyapatite, intertwined with softer collagen fibrils (Fratzl, 2008). The arrangement and structure of the fibrils and the ratio and relative orientation of mineral and protein phases determines the unique mechanical properties of the connective tissue (Claes et al., 1995; Martin and Boardman, 1993; Nalla et al., 2003; Wu and Herzog, 2002). Thus, the structure and organization of individual collagen fibrils contributes to the mechanical and functional properties of the tissue where it is found, such as the transparent cornea, elastic tendon, stiff bone, and soft cartilage (Fratzl, 2008).

Collagens are present in all multicellular organisms and in many tissues, including bone, tendon, cartilage, teeth, cornea, skin, and blood vessels (Fratzl, 2008). The structure of collagen molecules and fibrils has been studied extensively by X-ray diffraction and EM techniques (Fraser et al., 1987; Hodge and Petruska, 1963; Holmes, 1996; Orgel et al., 2006; Veis et al., 1967; Wess et al., 1998). The collagen molecule consists of 3 hydrogen bond-stabilized polypeptide strands and has a polar orientation directed from the amine (N)-terminus toward the carboxyl (C)-terminus. In collagen type I, these molecules self-assemble into fibrils, with a characteristic 67 nm periodicity along the fibril length arising from the stacking of the molecules. The fibrils maintain the N to C polarity of the molecules at the fibril ends, and are stabilized by covalent lysyl oxidase cross-linking (Bozec et al., 2007; Kadler et al., 1996).

In the framework of Wolff's law, bone remodels in response to mechanical stress to produce a structure best-suited to withstand the applied stress (Frost, 1990). How cells sense mechanical stimuli of different magnitudes, direction, and duration, however, is not fully understood (Papachroni et al., 2009). Thus, understanding the polar orientation of collagen may provide insight into the structure and biofunctional properties of these tissues. Several

techniques, including optical microscopy, EM, and AFM, have been applied to visualize the arrangement and alignment of collagen fibrils (Gale et al., 1995; Gotoh and Sugi, 1985; Kadler et al., 1996). Unlike EM techniques, which require dehydrated fibrils, AFM measurements allow tissues to be imaged in air, liquid, and physiologically relevant environments. Many studies have been undertaken to visualize the structure and to measure the mechanical properties of collagenous tissues and collagen fibrils using AFM, including the assembly of collagen (Gale et al., 1995), mechanical and viscoelastic properties (Minary-Jolandan and Yu, 2009a; Yang et al., 2008) and the effect of diseases such as diabetes on collagen ultrastructure (Odetti et al., 2000; Wang et al., 2003). Standard microscopy techniques, however, are not sensitive to the polar orientation of the molecules, the polar direction of a fibril, or the polar architecture of a tissue. Only with EM and immunolabeling has the N to C polar orientation of fibrils been determined in tissues (Kadler et al., 1996).

The presence of polar bonds in collagen fibrils gives rise to the piezoelectric properties reported in collagenous tissues (Fukada, 2000). Piezoelectricity is the linear coupling between mechanical strain and electric charge, and conversely, between electric field and deformation, and depends on crystal structure and polar orientation. Piezoelectricity in fibrils of type I collagen has further been attributed to the quasi hexagonal lateral packing of collagen molecules, although not all experimental evidence supports this (Berisio et al., 2001; Fratzl, 2008; Okuyama, 2008; Perumal et al., 2008; Prockop and Fertala, 1998). Piezoelectricity and related properties were first demonstrated in biological materials in 1941 (Martin, 1941) and ultimately, the piezoelectric effect was identified in a wide variety of biomaterials including bone, blood vessel walls, chitin, fibrin, cellulose, and DNA (Bazhenov, 1961; Fukada, 1955, 2000; Lemanov, 2000; Nalwa, 1995). The first published report on piezoelectricity in bone in 1957 (Fukada and Yasuda, 1957) sparked intense research on bone piezoelectricity (Fukada and Yasuda, 1964; Lang, 1966), and it was speculated that piezoelectricity could be responsible for the remodeling of calcified tissues (Bassett, 1968; Marino and Becker, 1970).

Piezoelectricity as a function of hydration has previously been investigated in the cornea and sclera from bovine and human sources (Ghosh et al., 1998; Jayasuriya et al., 2003a;

Jayasuriya et al., 2003b). These studies have confirmed the presence of piezoelectricity in the cornea and sclera and also demonstrate that the magnitude of the measured piezoelectric coefficient d_{31} increases with the degree of hydration of each tissue. Fourier transform infrared spectroscopy and wide-angle x-ray diffraction measurements have shown that collagen crystallinity increases with increasing hydration, highlighting the importance of the role of water in both the structure and functionality of collagen (Jayasuriya et al., 2003b). Furthermore, high piezoelectric anisotropy has been observed in these tissues (Jayasuriya et al., 2003a). In this regard, it would be desirable to probe piezoelectricity on the nanoscale to determine the origin of electromechanical coupling in these complex tissues. The piezoelectric nature of collagen allows the N to C polarity to be mapped using a voltage modulated AFM-based technique. Piezoresponse force microscopy (PFM) has been developed to probe piezoelectric and ferroelectric properties of ferroelectric materials and has been extended to piezoelectric semiconductors (Rodriguez et al., 2002), organic polymers (Rodriguez et al., 2007), and biological samples, including collagen (Harnagea et al., 2010; Minary-Jolandan and Yu, 2009b, 2009c; Rodriguez et al., 2006b; Sharma et al., 2011), a variety of connective tissues (Gruverman et al., 2007; Habelitz et al., 2007; Halperin et al., 2004; Kalinin et al., 2005, 2006b; Minary-Jolandan and Yu, 2010), polysaccharides (Binetti et al., 2009; Gruverman et al., 2006), and peptide nanostructures (Bdikin et al., 2012; Heredia et al., 2010; Kholkin et al., 2010). Recently, ferroelectricity was observed at the nanoscale in aortic arterial walls (Liu et al., 2012) and in crystalline γ-glycine (Heredia et al., 2012) demonstrating the importance of electromechanical coupling in biological systems, the implications of which are currently not understood.

Electromechanical coupling in piezoelectric biopolymers may play a role in, e.g., load-dependent bone remodeling. A preliminary step in determining this is to assess the piezoelectric properties of biological tissues, and in particular of the molecular polar order. The polar ordering is indicative of the sign of the piezoelectric coefficients, and thus may be responsible for any directionally dependent biofunctionality. Here, using PFM, we distinguish the molecular orientation of individual collagen fibrils and determine the polar architecture of

rat tail tendon and porcine eye tissues. This technique could be useful in understanding the role of polarity in materials properties and improve our current understanding of cell signaling and mechanotransduction.

2. Materials and methods

2.1 Collagen fibrils on glass slides preparation

Collagen type I from bovine Achilles tendon (Sigma-Aldrich) was swollen in 0.01 M hydrochloric acid for several hours at 0 °C. The solution was then homogenized for 10 min at 9500 RPM, filtered, diluted, and reconstituted in phosphate buffered saline (PBS) to a concentration of 10 μg/mL. 50 μL of the solution was pipetted onto a glass slide and allowed to incubate at room temperature for 10 minutes prior to rinsing in ultrapure water (18.2 $M\Omega cm^{-1}$ resistance, Millipore) to avoid salt crystal formation.

2.2 Rat tendon and porcine eye tissue sample preparation

Tendon specimens were harvested using a scalpel and removed with tweezers. The tendon was placed on a gold coated mica disk and allowed to dry in air following rinsing in ultrapure water. The dimensions of the tendon, measured via micrometer, were 440 ± 20 μm in diameter and 4.2 ± 0.02 mm in length. For the tendon cross-section, strands of fascicle were embedded in epoxy, cut transversely and polished in a 0.25 μm diamond slurry. The resulting cross-section diameter was measured to be 400 ± 20 μm. The cornea, sclera, and iris tissues were harvested from a pig and similarly embedded in epoxy, cut transversely, and polished. The dimensions of the cornea cross section was 1.88 ± 0.02 mm in length and 220 ± 20 μm in thickness; sclera dimensions were 1.28 ± 0.02 mm in length and 400 ± 20 μm in thickness and the iris dimensions were 4.33 ± 0.02 mm in length and 380 ± 20 μm in thickness.

2.3 Piezoresponse force microscopy

In PFM, a bias is applied to a conducting cantilever in contact mode AFM and the resulting tip deflection or torsion (lateral twisting of the cantilever) is measured. The tip torsion and

deflection provide information about the friction and topographic features of the sample, respectively, but also contain information about bias-induced sample deformations due to the converse piezoelectric effect, and a lock-in technique is used to distinguish between the two. The larger the piezoelectric coefficient of a material, the larger the deformation, and whether the deformation is in-phase or out-of-phase with the applied bias is related to the polar orientation (and the sign of piezoelectric coefficient) of the crystal, molecular assembly, or molecule. Thus, PFM provides information on the magnitude of the electromechanical coupling and the orientation of the material being investigated.

Here, PFM was implemented using an Asylum Research MFP-3D AFM equipped with Stanford Research Systems (SR830) and Zurich Instruments (HF2LI) lock-in amplifiers and a Tektronix (AGF320) function generator. To enhance the piezoelectric signal obtained during measurements, high-voltage PFM was used. An amplifier was constructed using an APEX model PA85 operational amplifier, which amplified the AC excitation signal with a gain of 10. A high voltage PFM Module (Asylum Research) with a gain factor of 22 was also used for some measurements.

During PFM experiments, the conductive AFM probe (DPE 18, Mikromasch) was in contact with the sample (typical imaging force 90 nN) and an AC bias (~20-40 V_{pp} at 22 kHz) was applied (Fig. 1A). If an out-of-plane piezoresponse was present, the tip deflects vertically (vertical arrow) resulting in a subsequent vertical deflection of the laser position on the photodetector. If a shear or in-plane piezoresponse was present, there would be a torsional movement of the cantilever (curved arrow) and a subsequent lateral movement of the laser on the photodetector. For collagen fibrils, the application of a bias perpendicular to the fibril axis (the length) results in a shear deformation, detectible via the torsion of the cantilever (Abplanalp et al., 1998). An AFM topography image of two collagen fibrils parallel to each other is shown in Fig. 1B. Overlaid on this image is the simultaneously captured LPFM phase image data. The top and bottom fibrils exhibit a 180° phase shift. In PFM, a 180° phase shift between two materials (or domains) signifies they are oscillating out of phase with each other and have opposite polar directions. Henceforth, bright phase (+90°) will be assigned to represent a fibril

which has an N to C polar direction pointing towards the right of the page and dark phase (-90°) denotes the N to C polarity pointing towards the left, which is highlighted with arrows on each phase image.

While quantitative measurements are possible, in this study, the focus is placed on the determination of the polar orientation of the tissues under investigation via PFM phase imaging. Both lateral and vertical PFM have been implemented (LPFM and VPFM, respectively).

Lateral PFM calibration was undertaken based on the geometry of the cantilever (Peter et al., 2005) using the equation $R = 4L/3h$, where L is the length of the cantilever, h is the combined height of the tip and cantilever thickness and R is the ratio between the out-of-plane sensitivity and the in-plane sensitivity. The frequency was chosen to be in a regime where it is thought that the tip will follow the lateral surface movements (Jesse et al., 2006). Vertical PFM was calibrated using a force curve on a hard surface before measurements to obtain the out-of-plane sensitivity.

3. Results and Discussion

PFM has been implemented to study the polar architecture of collagenous tissues. Each sample described above has been studied via PFM, revealing the polar orientation of the tissues at the fibrillar level.

3.1 PFM demonstration on an isolated collagen fibril

To demonstrate the principle of PFM on collagenous tissues, individual collagen fibrils have first been studied. As collagen is a shear piezoelectric, LPFM has been implemented to characterize the in-plane electromechanical properties of a single collagen fibril. A topography image of a single bent collagen fibril with a LPFM phase image overlay is shown in Fig. 1C. Due to the N to C polarity of collagen the bend in the fibril should result in a 180° shift in the LPFM phase signal at the bent region. The transition in the phase signal expected on either side of the bend is clearly evident, demonstrating the potential this technique has to map the polar orientation of

piezoelectric biomaterials. Without any modifications to the sample under investigation (e.g., staining, bleaching, etc.), the polar orientation of the biomaterial can be determined.

3.2 Polar orientation imaging of rat tail tendon and transversely cut rat tendon

Tendon comprises closely packed, highly aligned, parallel arrays of collagen fibrils, which connect muscle to bone. Tendon contains a small volume of proteoglycans and elastin and is enclosed by epitenon, a connective sheath (Kannus, 2000). An AFM deflection image of as-prepared rat tail tendon is shown in Fig. 2A. There is no fibrillar structure visible in this image, which suggests the surface of the tendon would need to be bleached in order to reveal fibrils underneath (Habelitz et al., 2002). The LPFM amplitude image (Fig. 2B) of the same area, however, confirms shear piezoelectricity in tendon. The piezoresponse in the image appears to originate from individual fibrils, demonstrating that piezoelectricity in tendon derives from collagen fibril piezoelectricity. The amplitude signal varies throughout the image, which is likely due to the fibrils having different depths resulting in varying magnitude of the amplitude signal. It is also possible that regions with lower signal have, e.g., more epitenon on the surface, which would effectively dampen the lateral signal. In addition to confirming piezoelectricity in tendon, the orientation of the fibrils can be visualized from a surface which has no visible collagen fibrils. The LPFM phase image in Fig. 2C reveals the polar ordering of the fibrils in the tissue. There is a predominant +90° phase in this image, but this is not an accurate representation and has resulted from the imaging conditions. The reasons for which are described in more detail below. Fig. 2D displays an AFM height image of a smaller scan area. In this image, fibrillar periodicity remains invisible. From the LPFM amplitude image (Fig. 2E) of the same area, however, fibrillar piezoresponse is evident with the “domains” having an average width of 73 nm ± 25 nm (n = 20), a domain being defined as an individual fibril or groups of fibrils with a uniform polarity. The widths of the “domains” in the image are of the same order to that of a single collagen fibril, indicating that the lateral piezoelectric signal originates from individual fibrils in the tendon. The LPFM phase image (Fig. 2F) of this region displays the anti-parallel polar ordering of the fibrils observed in Fig. 2C where each phase domain can be attributed to a

single collagen fibril. Since this observation is not discernible in the larger size scale PFM phase image, we assume we may need higher resolution/improved imaging conditions to resolve the phase domains of individual fibrils at this scan size. Each neighbouring fibril has an opposite polar orientation, an observation made before in fixed fascia tissue (Harnagea et al., 2010) where groups of fibrils exhibited opposite polar orientations, but not single fibrils, as in this case.

As PFM probes the surface of the material, additional PFM studies of rat tail tendon cross sections were undertaken to investigate if this observed anti-parallel polar ordering feature is present throughout the thickness of tendon tissue. VPFM is used on this sample as we are investigating the transverse cut of collagen fibrils, which have a non-zero d_{33} piezoelectric component (Fukada and Yasuda, 1964), giving rise to an out-of-plane piezoresponse in this setup. No clear periodic structure is visible in the topography image in Fig. 3A, given collagen fibrils align along the tendon axis with few aligning transversely, nor is there clear structure associated with cross-sectioned fibril ends at this scan size. The VPFM amplitude image is shown in Fig. 3B which confirms the presence of an out-of-plane piezoresponse. Similarly to Fig. 2B, a varying signal is observed throughout the image, with some bundles or domains having a larger signal. This could be due to fibrils present on the surface having different depths due to sample preparation or dehydration of the sample. It is important to note also that the maximum signal for the piezoelectric surface of d_{33} for collagen is at a 45° angle from the fibril axis (Kalinin et al., 2006b). While the values are based on macroscopic measurements (Fukada and Yasuda, 1964), they demonstrate the orientational dependence of the measured piezoelectric signal is non trivial. A smaller scan size AFM topography image (Fig. 3D) from a different area of the tissue again reveals few discernible details on the surface structure; however, in the deflection image (inset), there are small circular trenches (highlighted via white arrows) with an average diameter of 170 nm ± 56 nm (n = 15), which could correspond to the cross-section of individual or bundles of collagen fibrils. Fig. 3E displays a smaller scan size VPFM amplitude image of a region in (Fig. 3B). Piezoelectric domains in this image have an average width of 301 ± 131 nm corresponding to a bundle of ~ 2-4 fibrils. As a

high out-of-plane signal is observed in this image, it can be assumed that the orientation of the fibrils in this area are between 45° and orthogonal with respect to the page plane. The VPFM phase image (Fig. 3F) displays the orientation of the domains visible in Fig. 3B. The existence of domains here is significant as it demonstrates that the anti-parallel polar ordering which is present on the surface of tendon is translated throughout the thickness of the tissue. While little is known about the influence of piezoelectricity in biological systems or whether it plays a role in mechanotransduction, the observation of an anti-parallel polar ordering of collagen fibrils in native tissue may help shed light on these questions.

A histogram analysis is used in order to make a quantitative measure of the ratio of +90° and -90° pixels, which in turn represent the ratio of domains. Each pixel in the phase images is plotted in histogram form where two peaks, at +90° and -90°, are expected. The difference in intensity of these peaks combined with inspection of the AFM images gives an indication of the ratio of fibrils with a +90° polarity to those with a -90° polarity. A histogram is taken of the small scan size PFM phase image (Fig. 2F) of rat tail tendon, which is displayed in Fig. 4A. Here, there is a 9 % difference between the +90° and -90° peaks, illustrating that there is an almost equal amount of +90° polarity fibrils to -90° fibrils. The 'domains' of fibrils in the image from which this histogram is taken, however, have widths of approximately one individual fibril, demonstrating that an anti-parallel polar ordering phenomenon down to the fibrillar lever exists on the tendon surface.

The same histogram analysis is used for the cross-sectioned rat tail tendon sample to investigate if a similar polar ordering trend persists throughout the thickness of the tissue. Fig. 4B displays a histogram of the pixels in Fig. 3F. 42% more pixels represent fibrils with a polarity pointing out of the page (-90°) than fibrils with a polarity pointing into the page (+90°). While the difference in +90° fibrils and -90° fibrils is larger here than on the surface of tendon, the phase images and histograms demonstrate that there are significant populations of fibril domains with opposite polarity and that these exist throughout the thickness of tendon tissue.

3.3 Polar orientation imaging of sclera and cornea

The cornea and sclera comprise of the outer shell of the eye and are structured to withstand internal and external forces. Both primarily contain collagen fibrils, but many EM studies of the cornea and sclera have revealed that the collagen type and the distribution of fibrils are quite different in the two tissues (Komai and Ushiki, 1991). X-ray microscopy, EM, and AFM have shown that the sclera is composed of collagen fibrils of varying diameters, which organize in randomly oriented lamellae (thicknesses varying from 0.5 – 6 μm) resulting in the opaque characteristic of the sclera (Fullwood et al., 2011). The cornea, however, consists of highly organized lamellae consisting of aligned collagen fibrils of uniform diameter of 25 nm which contribute to the transparency of the tissue. The lamellae in the cornea all generally align along the tissue surface axis but form orthogonal to each other with the size of lamellae ranging from 0.2 – 2.5 μm (Komai and Ushiki, 1991; Polack, 1961).

To study the polar orientation of the sclera, both VPFM and LPFM have been implemented. Fig. 5A is an AFM height image of an area in the sclera displaying a region containing a boundary between three different lamellae. The dashed white line represents the boundary between the three lamellae and each lamella is numbered. Fig. 5D is an AFM tapping mode amplitude image from the black box highlighted in Fig. 5A. In this image the lamellae, labeled 2 and 3, exhibit the D-periodicity of type I collagen (circled). The fibrillar orientation is highlighted via double arrows. No D-periodic banding is visible in lamella 1 suggesting an absence of fibrils parallel to the cantilever axis here. Lamellae 2 and 3, for the given fibrillar orientations, would be expected to exhibit a high in-plane signal due to the shear piezoelectricity of collagen. This is confirmed from the LPFM amplitude image in Fig. 5B, where a high shear piezoresponse is observed in lamella 2 and 3. The fibrillar orientation within these two lamellae is recognizable in this image and follows the orientation of the fibrils highlighted in Fig. 5D. Piezoelectric domains of varying widths corresponding to fibrils/bundles of fibrils are visible in lamellae 2 and 3 which is consistent with previous studies of the sclera which state there a large variation in fibrillar widths in the sclera (Komai and Ushiki, 1991). From this image the average domain width is 393 nm ± 253 nm (n = 20). This large standard deviation would

suggest that the domain widths consist largely of bundles of fibrils. The fibrillar orientation in lamella 1 is more difficult to visualize from the LPFM amplitude image as it has a lower signal than the other two lamellae and has no recognizable surface features but exhibits a non-zero lateral piezoresponse. By directly comparing the LPFM amplitude image with the VPFM amplitude image (Fig. 5E), a more complete visualization of the fibrillar orientation can be seen. A low piezoelectric out-of-plane response is seen in lamella 2, as expected due to the high lateral signal present in Fig. 5B and the fibrils having an orientation almost perpendicular to the cantilever axis. However, a high response in the VPFM amplitude for lamella 3 is observed. This is most likely due to cantilever buckling as the orientation of the fibrils in this lamella is almost parallel to the cantilever axis. The high in-plane response for this lamella can transfer to an out-of-plane cantilever buckling in this orientation which has been studied before (Harnagea et al., 2010). Lamella 1, however, has a larger out-of-plane piezoresponse than the in-plane response seen in Fig. 5B. This would suggest that the collagen fibrils in this lamella are actually orthogonal to the long axis of the cantilever, resulting in this high out-of-plane response. The domains in this lamella are 507 nm ± 288 nm (n = 3) in width, indicating the domains represent bundles of fibrils.

By studying the LPFM and VPFM phase images, mapping the polar ordering of the tissue is possible. The N to C polarity of collagen is assigned and labeled in the image. As deduced from the LPFM amplitude image in Fig. 5B, the lamellae 2 and 3 contain fibrils in parallel plane with the cantilever axis; therefore LPFM phase image (Fig. 5C) will be used to describe the polar orientation of these lamellae. Fibrils in the lamella 2 predominantly have a polar direction pointing to the right of the image with a small number of domains of fibrils having a polarity pointing to the left of the page. Lamella 3 has a predominant polar direction which is opposite to lamella 2, again with a small number of fibrils having an opposite polarity. From comparison of the LPFM and VPFM amplitude images as described above, there is evidence that lamella 1 has fibrils which are oriented in the plane orthogonal to the page plane and cantilever axis, therefore the VPFM phase image in Fig. 5F will be used to describe its polar ordering. The bright regions in this lamella correspond to fibrils with a +90° polarity (⊗) pointing into the page, and

the dark regions correspond to fibrils with a -90° polarity (double circle) pointing out of the page. In comparison to the LPFM phase images from rat tendon, there appears to be quite different polar architectures between the sclera and tendon. In the sclera, there is no evidence of anti-parallel polar ordering between fibrils; rather it exists only between domains consisting of bundles of fibrils.

An AFM topography image of a large area of the cornea is displayed in Fig. 6A. A banding structure is visible (examples outlined via dashed white lines) in this image of different widths which likely corresponds to the well known lamellar structure of the cornea. However, it is difficult to deduce the orientation of the collagen fibrils within these lamellae from the height image. VPFM has been implemented to investigate any differences in the out-of-plane piezoresponse between lamellae which would shed some light on the orientation of collagen fibrils in these lamellae. In the VPFM amplitude image (Fig. 6B), there is certainly a visible difference in the out-of-plane piezoresponse between the different lamellae. Lamellae which are visible both in the topography image and in the VPFM amplitude and phase images are highlighted via dashed lines. Each neighbouring lamella appears to either have a strong and uniform out-of-plane signal or a heterogeneous out-of-plane signal consisting of areas with both weak and strong signals. The polar orientation of the lamella can be investigated through the VPFM phase image (Fig. 6C). The lamellar structure visible in both the topography and VPFM amplitude image is still discernible in the phase image. The lamellae which had a strong, uniform piezoresponse in Fig. 6B also have a uniform polarity, pointing into the page. The lamellae which showed a heterogeneous piezoresponse consist of regions with opposite polarity. The topography of a smaller scan size area is displayed in Fig. 6D, showing more clearly the distinct lamellar structure. The lamellae appear to have quite varied widths (1 µm ± 400 nm; n = 15), which previous studies have also reported (Komai and Ushiki, 1991). Even with a smaller scan size however, the orientation of the collagen fibrils is not easily visualized. In the VPFM amplitude image, again the lamellar structure is evident with every neighbouring lamella having a high out-of-plane piezoresponse. When compared with the VPFM phase image of the same area, a similar trait is observed to that seen in Fig 6C. Lamellae which exhibit a high out-

of-plane response appear to comprise collagen fibrils with a uniform polar orientation and lamellae with a heterogeneous piezoresponse contains domains of fibrils exhibiting opposite polar orientations. To study this structure more conclusively, both lateral and vertical PFM have been implemented at a boundary between two lamellae.

An AFM topography image showing the boundary between two lamellae in the cornea is displayed in Fig. 7A. The D-periodicity of collagen is visible in the upper lamella, whereas no periodicity is evident in the bottom lamella. Round raised features are visible in the bottom lamella however, in the AFM deflection image (Fig. 7D). Shear piezoelectricity is investigated via the LPFM amplitude image (Fig. 7B), which shows there is a significant difference in the in-plane piezoresponse between the two lamellae. The top lamella has a large in-plane piezoresponse signal displaying domains of fibrils with an average width of 267 nm ± 171 nm (n = 20). This indicates the piezoelectric domains consist of bundles of fibrils as the reported collagen fibril width in the cornea is a uniform 25 nm. From the high in-plane signal from the top lamella and the D-periodic fibrils visible in topography, it can be deduced that the orientation of collagen fibrils in this lamella are parallel to the page plane. The bottom lamella, in contrast, has minimal in-plane piezoresponse. In the corresponding LPFM phase image (Fig. 7C), the polar orientation of each piezoelectric domain observed from Fig. 7B can be visualized. VPFM is used in order to determine the orientation of collagen in the bottom lamella. A high out-of-plane signal would suggest that there are collagen fibrils orthogonal to the top lamella. A low out-of-plane piezoresponse would be expected in the top lamella as shear piezoelectricity has been verified in this lamella from the LPFM image. This assumption is validated in the VPFM image (Fig. 6E) as the top lamella gives minimal out-of-plane signal. There is a high out-of-plane signal from the bottom lamella however, which would suggest the presence of collagen fibrils pointing out of the page where the domains appear to be arranged in bundles of fibrils. However, if we assume the collagen orientation in the bottom lamella is actually in-plane but oriented perpendicular to the top lamella, an out-of-plane piezoresponse would be expected for this cantilever-collagen orientation. In this case, the shear deformation of collagen would give rise to an out-of-plane piezoresponse in the form of cantilever buckling as described in the sclera above. It is important

to note, however, that if this orientation was the case, we would expect to see an in-plane piezoresponse from the bottom lamella in Fig. 7B as the cantilever would still be sensitive to the induced torsional twisting as seen in Fig. 5B (Harnagea et al., 2010). While there is a small possibility that this may be the actual collagen configuration, this image reveals the importance of taking all possible cantilever-collagen orientations into consideration. For this case it would be ideal to rotate the sample 90° in order to verify this lamella has only an out-of-plane signal (Kalinin et al., 2006a). The structure of the surface of this lamella however does suggest that the fibrils are orthogonal to the top lamella. The surface here comprises round raised features, more easily visible in the AFM deflection image (Fig. 7D), which are 150 nm ± 28 nm in diameter. While fibrils in the cornea have been shown to have a uniform diameter of 25 nm, it is plausible that these raised features could be the ends of bundles of fibrils, or that they are the correct size but appear larger in diameter due to tip broadening effects. For these reasons, we strongly believe that the bottom lamella is orthogonal to the top lamella. The VPFM phase image in Fig. 7F reveals that each neighboring domain present in the bottom lamella exhibits an opposite polar orientation. The orientation of the domains in this lamella is very similar to that which is seen in the cross section of tendon (Fig. 3F), where a layering of the domains is observed.

These images show conclusively that collagen in the sclera and cornea is indeed piezoelectric, consists of interwoven and orthogonal lamellae and that the origin of piezoelectricity in the cornea and sclera is due to collagen fibrils. In addition to these observations, the polar orientation of collagen fibrils in the sclera has been visualized. While the presence of a polar direction in collagen fibrils has been studied previously, the organization of the polar orientation of fibrils in native tissues has not been considered in any previous study. No uniform polarity is observed in the sclera or cornea, all lamellae imaged revealed an anti-parallel polar ordering between domains consisting of bundles of collagen fibrils.

3.4 Polar orientation imaging of iris

The iris controls the size of the pupil, and hence the amount of light entering the eye. The stroma contains collagen fibrils interwoven around blood vessels and the iris sphincter (Muroň and Pospíšil, 2000). Both VPFM and LPFM have been used to study porcine iris. The iris stroma contains collagen fibrils interwoven around blood vessels and the iris sphincter which is the region under investigation in this study. Fig. 8A is a large AFM topography image displaying the surface of the iris stroma. Fibrils are visible and exposed on the surface even with no surface treatment. The D-periodicity of type I collagen can be observed in the image and the fibrils have a uniform orientation. The average fibril width measured from these images is 205 nm ± 65 nm (n = 20). This fibrillar width is much larger than that reported for the cornea and the sclera. Fig. 8B displays the LPFM amplitude image, where shear piezoelectricity is confirmed. This is expected as the collagen fibrils are oriented perpendicular to the long axis of the cantilever, thus the in-plane piezoresponse is maximized. For this reason, no vertical signal will be measured, hence only LPFM images are used for investigation of the iris. The in-plane piezoelectric 'domains' of fibrils have an average width of 400 nm ± 207 nm (n = 20), indicating that each domain consists of ~ 1-4 fibrils. The LPFM phase image of this area maps the polar orientation of the iris as shown in Fig. 8C where the polar orientation of each domain is visible. Fig. 8D is an AFM topography image of smaller scan area within Fig. 8A highlighting the individual fibrils. They all show evidence of the 67 nm D-periodicity of type I collagen, demonstrating that the collagen fibrils are completely exposed on the surface. The small scan size LPFM amplitude image (Fig. 8E) directly compared with the topography allows us to distinguish that the piezoelectric domains consist of multiple fibrils. While the orientation of the fibrils is visible from the topography image, the LPFM amplitude image also provides information on the orientation. By directly comparing Fig 8D with Fig 8E, it can be seen that the piezoelectric domains consist of both a number of fibrils (large white oval) and single fibrils (small white oval). The corresponding LPFM phase image allows for the visualization of the N to C polarity of the fibrils, which in this case organize in domains of opposite polarities. The white circle highlights a region where fibrils are visibly interwoven in between each other. This is a

characteristic previously reported in the iris (Muroň and Pospíšil, 2000). To further confirm D-periodicity in the iris, a 2D FFT analysis of a collagen fibril was undertaken from an area (highlighted by the white box) in the AFM deflection image (Fig. 8G) containing a D-periodic collagen fibril. The resulting FFT (Fig. 8H) yields two main peaks which correspond to the axial spacing of collagen type I (labeled) and higher harmonics at a lower intensity (Wallace et al., 2011). The line profile shown in Fig. 8I is taken from the area highlighted by red line in Fig. 8D. This profile also confirms the presence of the 67 nm D-periodic banding of type I collagen with an average D-period of 66.2 ± 2.3 nm (n=5). Given the presence of D-periodic fibrils on the iris surface, which form domains of opposite polarities, iris stroma could be a suitable substrate to investigate the role of collagen polar ordering on cellular interactions in tissues.

4. Conclusion

While most microscopy techniques reveal information about alignment of collagen fibrils in connective tissues, the polar orientation of the fibrils, which may have implications for cell signaling, is not visible. Piezoresponse force microscopy has been employed to obtain information on both the polar orientation and the electromechanical properties of collagen fibrils in native rat tail tendon, transversely cut rat tail tendon, and porcine cornea, sclera, and iris tissues. Piezoelectricity has been confirmed in all tissues studied, emphasizing that piezoelectricity is a functional property in all collagenous tissues. By combining vertical and lateral PFM, the polar architecture in tissues can be visualized. Interestingly, no uniform polarity has been observed in any tissue studied. Rat tendon shows evidence of anti-parallel polar ordering down to the fibrillar level, which has been confirmed to persist partially through the thickness of the tissue by studying the cross section of rat tendon. PFM of interwoven and orthogonal lamellae within the cornea and sclera reveals that fibrils form piezoelectric domains consisting of bundles of fibrils exhibiting opposite polar orientations. These results show that collagen fibrils in natural and unmodified tissues form piezoelectric domains with anti-parallel polar orientations. There is no expectation that collagen fibrils will assemble to have either a unipolar orientation or to form piezoelectric domains. While no unipolar orientation was seen

in any tissue studied, domains of different size scales were observed in every tissue. It seems plausible to suggest that this observation is relevant for understanding mechanical and biofunctional properties of connective tissues. PFM has been shown to be a useful tool for characterizing tissues without the need for intensive sample preparation, giving information on collagen orientation and additional information on the polar orientation. PFM has previously been demonstrated in liquid environments on model systems, suggesting the possibility of carrying out similar measurements in physiological environments (Rodriguez et al., 2006a). The technique can be applied to any biological material containing piezoelectric biopolymers or polysaccharides. With recent discoveries of ferroelectricity in biological systems (Heredia et al., 2012; Liu et al., 2012) and the possibility of utilizing piezoelectricity in biosystems for piezoelectric energy generation (Lee at al., 2012), it is becoming more apparent that electromechanical coupling is of significant importance in the functionality of biosystems and for applications in biotechnology.

Acknowledgements

This publication has emanated from research conducted with the financial support of Science Foundation Ireland under grant number SFI10/RFP/MTR2855 and UCD Research. The authors would like to acknowledge the support of S.P. Jarvis and also J.I. Kilpatrick and S.H. Loh (UCD) for help with the electronics used in this project, and Dr. Jay Stewart (UCSF) for providing the porcine cornea. The authors are also grateful to Asylum Research UK for access to a high voltage PFM module.

References

Abplanalp, M., Eng, L.M., Günther, P., 1998. Mapping the domain distribution at ferroelectric surfaces by scanning force microscopy. App. Phys. A. 66, 231–234.

Bassett, C.A.L., 1968. Biologic significance of piezoelectricity. Calc. Tiss. Res. 1, 252–272.

Bazhenov, V.A., 1961. Piezoelectric properties of wood. Consultant Bureau Enterprise Inc., New York.

Bdikin, I., Bystrov, V., Kopyl, S., Lopes, R.P.G., Delgadillo, I. et al., 2012. Evidence of ferroelectricity and phase transition in pressed diphenylalanine peptide nanotubes. Appl. Phys. Lett. 100, 043702.

Berisio, R., Vitagliano, L., Mazzarella, L., Zagari, A., 2001. Crystal structure of a collagen-like polypeptide with repeating sequence Pro-Hyp-Gly at 1.4 Å resolution: Implications for collagen hydration. Biopolymers. 56, 8–13.

Binetti, V.R., Schiffman, J.D., Leaffer, O.D., Spanier, J.E., Schauer, C.L., 2009. The natural transparency and piezoelectric response of the greta oto butterfly wing. Integr. Biol. 1, 324–329.

Bozec, L., Van der Heijen, G., Horton, M., 2007. Collagen fibrils: Nanoscale ropes. Biophys. J. 92, 70–75.

Buehler, M.J., 2006. Nature designs tough collagen: Explaining the nanostructure of collagen fibrils. Proc. Natl. Acad. Sci. 103, 12285–12290.

Claes, L.E., Wilke, H.J., Kiefer, H., 1995. Osteonal structure better predicts tensile strength of healing bone than volume fraction. J. Biomech. 28, 1377–1385.

Dunlop, J.W.C., Fratzl, P., 2010. Biological composites. Annu. Rev. Mater. Res. 40, 1–24.

Fraser, R.D.B., MacRae, T.P., Miller, A., 1987. Molecular packing in type I collagen fibrils. J. Mol. Biol. 193, 115–125.

Fratzl, P., 2008. Collagen structure and mechanics. Springer, New York.

Frost, H.M., 1990. Skeletal structural adaptations to mechanical usage (SATMU): 1. Redefining Wolffs law: The bone modeling problem. Anat. Rec. 226, 403–413.

Fukada, E., 1955. Piezoelectricity of wood. J. Phys. Soc. Jpn. 10, 149–154.

Fukada, E., 2000. History and recent progress in piezoelectric polymers. IEEE Trans. Ultrason. Ferroelectr. Freq. Control. 47, 1277–1290.

Fukada, E., Yasuda, I., 1957. On the piezoelectric effect of bone. J. Phys. Soc. Jpn. 12, 1158–1162.

Fukada, E., Yasuda, I., 1964. Piezoelectric effects in collagen. Jpn. J. Appl. Phys. 3, 117–121.

Fullwood, N.J., Martin, F.L., Bently, A.J., Lee, J.P., Lee, S.J., 2011. Imaging sclera with hard X-ray microscopy. Micron. 42, 506–511.

Gale, M., Pollanen, M.S., Markiewicz, P., Goh, M.C., 1995. Sequential assembly of collagen revealed by atomic force microscopy. Biophys. J. 68, 2124–2128.

Ghosh, S., Mei, B.Z., Lubkin, V., Scheinbeim, J.I., Newman, B.A., et al., 1998. Piezoelectric response of scleral collagen. J. Biomed. Mater. Res. 39, 453–457.

Gotoh, T., Sugi, Y., 1985. Electron-microscopic study of the collagen fibrils of the rat tail tendon as revealed by freeze-fracture and freeze-etching techniques. Cell. Tissue. Res. 240, 529–534.

Gruverman, A., Rodriguez, B.J., Kalinin, S.V., 2006. Nanoscale electromechanical and mechanical imaging of butterfly wings by scanning probe microscopy. J. Scann. Probe. Micros. 1, 74–78.

Gruverman, A., Wu, D., Rodriguez, B.J., Kalinin, S.V., Habelitz, S., 2007. High-resolution imaging of proteins in human teeth by scanning probe microscopy. Biochem. Biophys. Res. Comm. 352, 142–146.

Habelitz, S., Balooch, M., Marshall, S.J., Balooch, G., Marshall G.W., 2002. In situ atomic force microscopy of partially demineralized human dentin collagen fibrils. J. Struct. Bio. 138, 227–236.

Habelitz, S., Rodriguez, B.J., Marshall, S.J., Marshall, G.W., Kalinin, S.V., et al., 2007. Peritubular dentin lacks piezoelectricity. J. Dent. Res. 86, 908–911.

Halperin, C., Mutchnik, S., Agronin, A., Molotskii, M., Urenski, P., et al., 2004. Piezoelectric effect in human bones studied in nanometer scale. Nano Lett. 4, 1253–1256.

Harnagea, C., Vallières, M., Pfeffer, C.P., Wu, D., Olsen, B.R., et al., 2010. Two-dimensional nanoscale structural and functional imaging in individual collagen type I fibrils. Biophys. J. 98, 3070–3077.

Heredia, A., Bdikin, I.K., Kopyl, S., Mishina, E., Semin, S., et al., 2010. Temperature-driven phase transformation in self-assembled diphenylalanine peptide nanotubes. Fast Track Communcation. 42, 462001.

Heredia, A., Meunier, V., Bdikin, I.K., Gracio, J., Balke, N., et al., 2012. Nanoscale ferroelectricity in crystalline γ-glycine. Adv. Funct. Mater. *In Press.*

Hodge, A.J., Petruska, J.A., 1963. Recent studies with the electron microscope on ordered aggregates of the tropocollagen molecule. In Aspects of protein structure. Ramachandran, G.N., editor. Academic press, New York. 289–300.

Holmes, D.F., 1996. Mass mapping of extracellular matrix assemblies. Biochem. Soc. Trans. 23, 720–725.

Jayasuriya, A.C., Ghosh, S., Scheinbeim, J.I., Lubkin, V., Bennett, G. et al., 2003a. A study of piezoelectric and mechanical properties of the human cornea. Biosens. Bioelectron. 18, 381–387.

Jayasuriya, A.C., Scheinbeim, J.I., Lubkin, V., Bennett, G., Kramer, P., 2003b. Piezoelectric and mechanical properties in bovine cornea. J. Biomed. Mater. Res. A. 66, 260–265.

Jesse, S., Baddorf, A.P., Kalinin, S.V., 2006. Dynamic behaviour in piezoresponse force microscopy. Nanotechnology. 17, 1615–1628.

Ji, B., Gao, H., 2004. Mechanical properties of nanostructure of biological materials. J. Mech. Phys. Solids. 52, 1963–1990.

Kadler, K.E., Holmes, D.F., Trotter, J.A., Chapman, J.A., 1996. Collagen fibril formation. Biochem. J. 316, 1–11.

Kalinin, S.V., Rodriguez, B.J., Jesse, S., Shin, J, Baddorf, A., et al., 2006a. Vector piezoresponse force microscopy. Microscopy and Microanalysis. 12, 206–220.

Kalinin, S.V., Rodriguez, B.J., Jesse, S., Thundat, T., Gruverman, A., 2005. Electromechanical imaging of biological systems with sub-10 nm resolution. Appl. Phys. Lett. 87, 053901.

Kalinin, S.V., Rodriguez, B.J., Shin, J., Jesse, S., Grichko, V., et al., 2006b. Bioelectromechanical imaging by scanning probe microscopy: Galvani's experiment on the nanoscale. Ultramicroscopy. 106, 334–340.

Kannus, P., 2000. Structure of the tendon connective tissue. Scand J Med Sci Sports. 10, 312–320.

Kholkin, A., Amdursky, N., Bdikin, I., Gazit, E., Rosenman, G., 2010. Strong piezoelectricity in bioinspired peptide nanotubes. ACS Nano. 4, 610–614.

Komai, Y., Ushiki, T., 1991. The three-dimensional organization of collagen fibrils in the human cornea and sclera. Invest. Opthalmol. Vis. Sci. 32, 2244–2258.

Lang, S.B., 1966. Pyroelectric effect in bone and tendon. Nature. 212, 704–705.

Lee, B.Y., Zhang, J., Zueger, C., Chung, W.J., Yoo, S.Y. et al., 2012. Virus-based piezoelectric energy generation. Nature Nanotech. *In Press.*

Lemanov, V.V., 2000. Piezoelectric and pyroelectric properties of protein amino acids as basic materials of soft state physics. Ferroelectrics. 238, 211–218.

Liu, Y., Zhang, Y., Chow, M.J., Chen, Q.N., Li, J. 2012. Biological ferroelectricity uncovered in aortic walls by piezoresponse force microscopy. Phys. Rev. Lett. 108, 078103.

Marino, A.A., Becker, R.O., 1970. Piezoelectric effect and growth control in bone. Nature. 228, 473–474.

Martin, A.J.P., 1941. Tribo-electricity in wool and hair. Proc. Phys. Soc. 53, 186.

Martin, R.B., Boardman, D.L., 1993. The effects of collagen fiber orientation, porosity, density, and mineralization on bovine cortical bone bending properties. J. Biomech. 35, 1047–1054.

Minary-Jolandan, M., Yu, M.F., 2009a. Nanomechanical heterogeneity in the gap and overlap regions of type I collagen fibrils with implications for bone heterogeneity. Biomacromolecules. 10, 2565–2570.

Minary-Jolandan, M., Yu, M.F., 2009b. Nanoscale characterization of isolated individual type I collagen fibrils: polarization and piezoelectricity. Nanotechnology. 20, 1–6.

Minary-Jolandan, M., Yu, M.F., 2009c. Uncovering nanoscale electromechanical heterogeneity in the subfibrillar structure of collagen fibrils responsible for the piezoelectricity of bone. ACS Nano. 3, 1859–1863.

Minary-Jolandan, M., Yu, M.F., 2010. Shear piezoelectricity in bone at the nanoscale. Appl. Phys. Lett. 97, 153127.

Muroň, A, Pospíšil, J., 2000. The human iris structure and its usages. Acta Univ. Palacki. Olomuc. 39, 87–95.

Nalla, R.K., Kinney, J.H., Ritchie, R.O., 2003. Effect of orientation on the in vitro fracture toughness of dentin: the role of toughening mechanisms. Biomaterials. 24, 3955–3968.

Nalwa, H.S., 1995. Ferroelectric polymers: chemistry, physics and applications. Dekker, New York.

Odetti, P., Argano, I., Rolandi, R., Garibaldi, S., Valentini, S., et al., 2000. Scanning force microscopy reveals structural alterations in diabetic rat collagen fibrils: role of protein glycation. Diabetes. Metab. Res.Rev. 16, 74–81.

Okuyama, K., 2008. Revisiting the molecular structure of collagen. Connective Tissue Research. 49, 299–310.

Orgel, J.P.R.O., Irving, T.C., Miller, A., Wess, T.J., 2006. Microfibrillar structure of type I collagen in situ. Proc. Natl. Acad. Sci. 103, 9001–9005.

Papachroni, K.K., Karatzas, D.N., Papavassiliou, K.A., Basdra, E.K., Papavassiliou, A.G., 2009. Mechanotransduction in osteoblast regulation and bone disease. Trends. Molec. Med. 15, 208–216.

Perumal, S., Antipova, O., Orgel, J.P.R.O., 2008. Collagen fibril architecture, domain organization, and triple-helical conformation govern its proteolysis. Proc. Natl. Acad. Sci. 105, 2824–2829.

Peter, F., Rüdiger, A., Waser, R., Szot, K., 2005. Comparison of in-plane and out-of-plane optical amplification in AFM measurements. Rev. Sci. Instrum. 76, 046101.

Polack, F.M., 1961. Morphology of the cornea. Am. J. Ophthalmol. 51, 179–184.

Prockop, D.J., Fertala, A., 1998. The collagen fibril: The almost crystalline structure. J. Struct. Bio. 122, 111–118.

Rodriguez, B.J., Gruverman, A., Kingon, A.I., Nemanich, R.J., Ambacher, O., 2002. Piezoresponse force microscopy for polarity imaging of GaN. Appl. Phys. Lett. 80, 4166.

Rodriguez, B.J., Jesse, S., Kalinin, S.V., Kim, J., Ducharme, S., et al., 2007. Nanoscale polarization manipulation and imaging of ferroelectric Langmuir-Blodgett polymer films. Appl. Phys. Lett. 90, 122904.

Rodriguez, B. J., Jesse, S., Baddorf, A.P., Kalinin, S.V., 2006a. High resolution electromechanical imaging of ferroelectric materials in a liquid environment by piezoresponse force microscopy. Phys. Rev. Lett. 96, 237602.

Rodriguez, B.J., Kalinin, S.V., Shin, J., Jesse, S., Grichko, V., et al., 2006b. Electromechanical imaging of biomaterials by scanning probe microscopy. J. Struct. Bio. 153, 151–159.

Sharma, P., Dong, W., Shashi, P, Reece, .J., Ducharme, S., et al., 2011. Orientational imaging in polar polymers by piezoresponse force microscopy. J. Appl. Phys. 110, 052010.

Veis, A., Anesey, J., Mussell, S., 1967. A limiting microfibril model for the three-dimensional arrangement within collagen fibres. Nature. 215, 931–934.

Wallace, J.M., Orr, B.G, Marini, J.C., Banaszak, M.M., 2011. Nanoscale morphology of type I collagen is altered in the brtl mouse model of osteogenesis imperfecta. J. Struct. Bio. 173, 146–152.

Wang, H., Layton, B.E., Sastry, A.M., 2003. Nerve collagens from diabetic and nondiabetic Sprague-Dawley and biobreeding rats: an atomic force microscopy study. Diabetes. Metab. Res. Rev. 19, 288–298.

Wess, T.J., Hammersley, A., Wess, A., Miller, A., 1998. Molecular packing of type I collagen in tendon. J. Mol. Biol. 275, 255–267.

Wu, J.Z., Herzog, W., 2002. Elastic anisotropy of articular cartilage is associated with the microstructures of collagen fibers and chondrocytes. J. Biomech. 35, 931–942.

Yang, L., Van der Werf, K.O., Fitie, C.F.C., Bennink, M.L., Dijkstra, P.J. et al., 2008. Mechanical properties of native and cross-linked type I collagen fibrils. Biophys. J. 94, 2204–2211.

Figure Captions

Fig. 1 LPFM and VPFM schematic with examples of polar orientational imaging of collagen fibrils. (A) Schematic of LPFM and VPFM operation. (B) 3D surface plot of an AFM topography image of two parallel collagen fibrils with simultaneously captured LPFM phase data overlaid. (C) 3D surface plot of an AFM topography image of a collagen fibril bent around with LPFM phase data overlaid.

Fig. 2 PFM images of rat tail tendon surface. (A) AFM topography image of tendon surface, inset shows cantilever orientation. Scan direction is parallel to the tissue long axis. (B) LPFM amplitude image of same area as (A) with corresponding scale bar. (C) LPFM phase image displaying polar orientation of fibrils underneath the surface. (D) AFM topography image of a smaller area of tendon obtained from a different location. (E) LPFM amplitude image and (F) LPFM phase image of this area. Scale bar for (A) – (C) is 2 μm, (E) – (G) is 200 nm. Z-scale bar for (A) is 400 nm and (D) is 130 nm.

Fig. 3 PFM images of a cross section of rat tail tendon. (A) AFM topography image of cross section surface. (B) VPFM amplitude and (C) VPFM phase image of area in (A). (D) AFM topography image of smaller area in (A), inset is AFM deflection image of same area as (D). White arrows highlight areas corresponding to trenches. (E) VPFM amplitude and (F) VPFM phase image of same area as in (D). Scale bar for (A) – (C) is 2 μm, (D) – (F) is 200 nm. Inset in (E) scale bar is 200 nm. Z-scale bar for (A) is 500 nm and (D) 120 nm.

Fig. 4 Phase histograms taken from small scale LPFM images from the surface of rat tendon and cross-sectioned rat tail tendon. The histogram in (A) is taken from phase image in Fig. 2F representing a ratio of opposite polarizations of fibrils in a rat tendon image. The histogram in (B) is taken from Fig. 3F representing the ratio of opposing polarities for cross sectional rat tendon.

Fig. 5 PFM images of porcine sclera. (A) AFM topography image displaying boundary between three lamellae highlighted via dashed white line. (B) LPFM amplitude and (C) LPFM phase image of area in (A). (D) AFM tapping mode amplitude image (zoom in from black box in (A)) with evidence (circled) of D-periodic fibrils on surface. Double white arrows represent fibrillar orientation. (E) VPFM amplitude and (F) VPFM phase image of area in (E). Scale bar for (A) – (C) and (E) – (F) is 1 μm. Scale bar for (D) is 500 nm. Z-scale bar for (A) is 250 nm.

Fig. 6 PFM image of porcine cornea. (A) AFM topography image displaying several lamellae arranged in rows highlighted by dashed white lines. (B) VPFM amplitude and (C) VPFM phase images of same large scan size area in (A). (D) is a smaller scan size AFM topography image in the cornea. (E) and (F) are the corresponding VPFM amplitude and phase images, respectively, from the area in (D). Scale bar for (A) to (C) is 2 μm, scale bar for (D) to (F) is 1 μm. Z-scale bar for (A) is 100 nm and (D) is 80 nm.

Fig. 7 PFM images of a boundary between two lamellae in porcine cornea. (A) AFM topography image displaying the boundary. (B) LPFM amplitude and (C) LPFM phase image of area in (A). (D) AFM deflection image of same area in (A) revealing D-periodic fibrils in top lamella. (E) VPFM amplitude and (F) VPFM phase image. Scale bar for all images is 500 nm. Z-scale for (A) is 60 nm.

Fig. 8 PFM images of porcine iris. (A) AFM topography image of iris surface revealing exposed collagen fibrils. (B) LPFM amplitude and (C) LPFM phase image of area in (A). (D) AFM topography image of smaller area taken from (A). (E) LPFM amplitude and (F) LPFM phase image from area in (E). (G) AFM deflection image of area in (D). (H) 2D FFT taken from area highlighted by white box in (G). (I) Line profile taken from red line in (D) displaying the D-banding of collagen. Scale bar for (A) – (C) is 5 µm, (D) – (G) is 1 µm. Z-scale for (A) is 800 nm and for (D) is 150 nm.

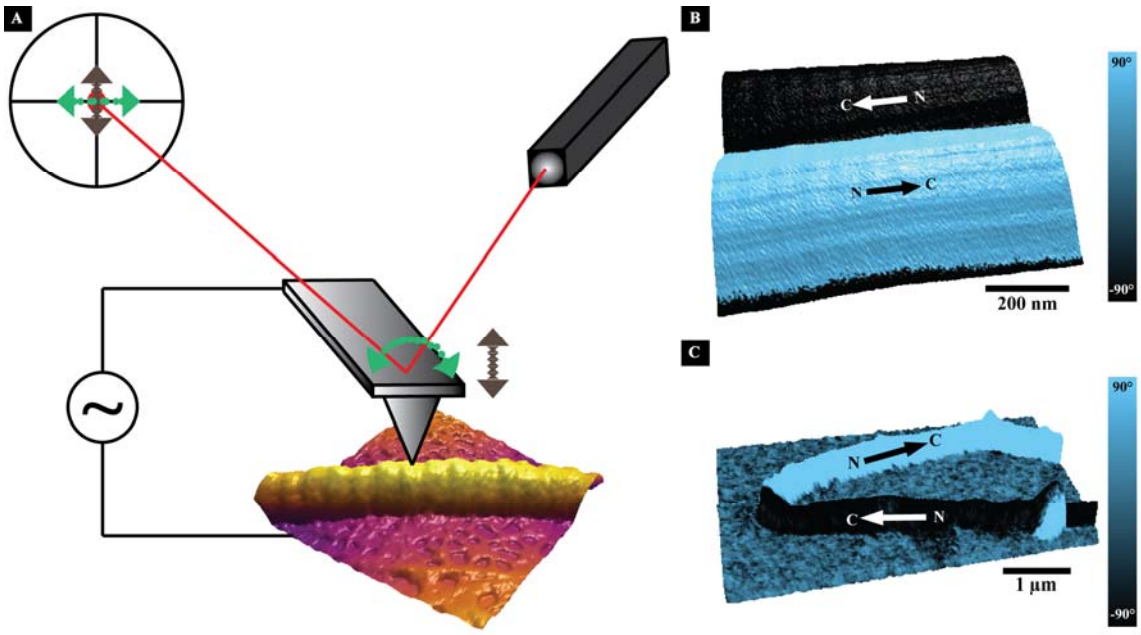

Denning et al. Figure 1

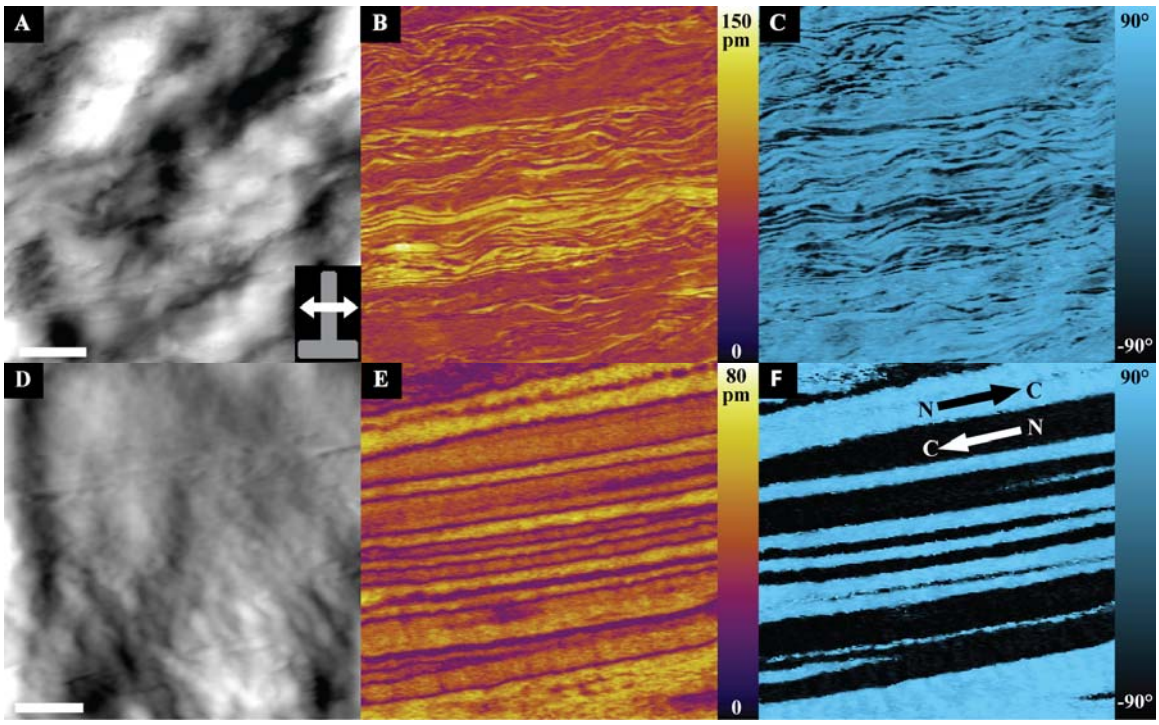

Denning et al Figure 2

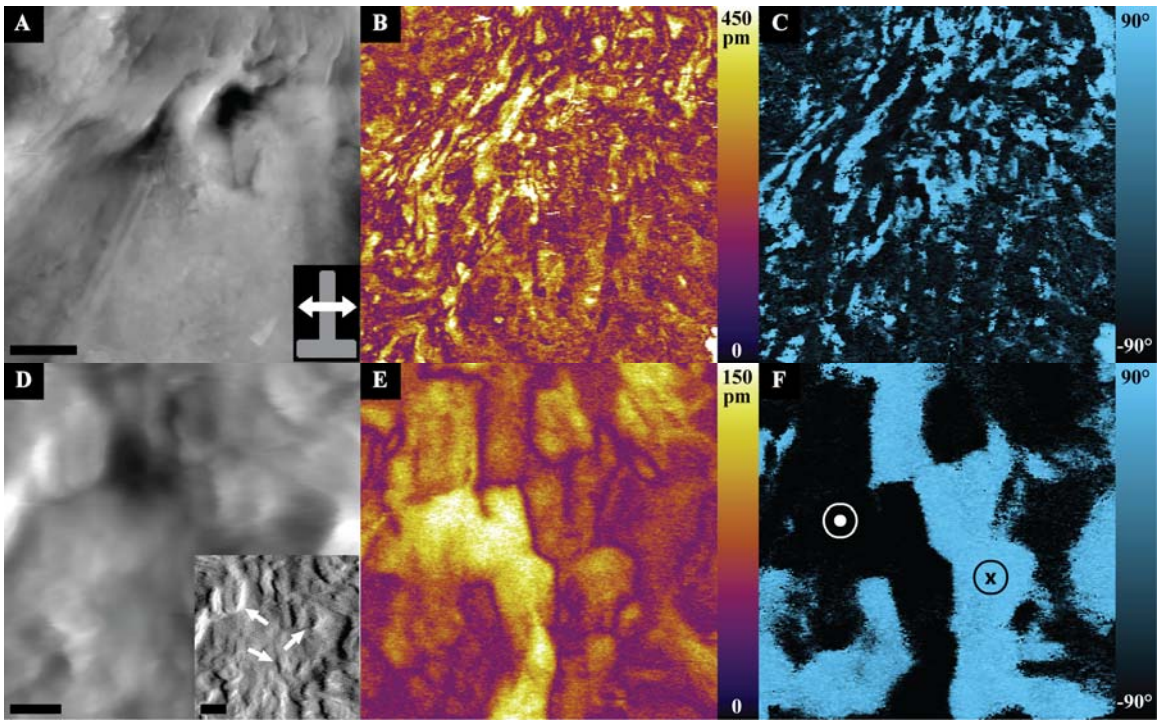

Denning et al Figure 3

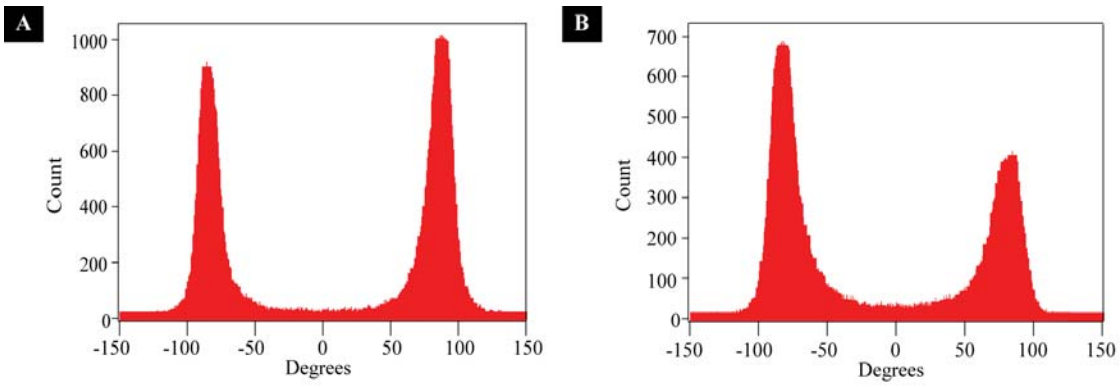

Denning et al Figure 4

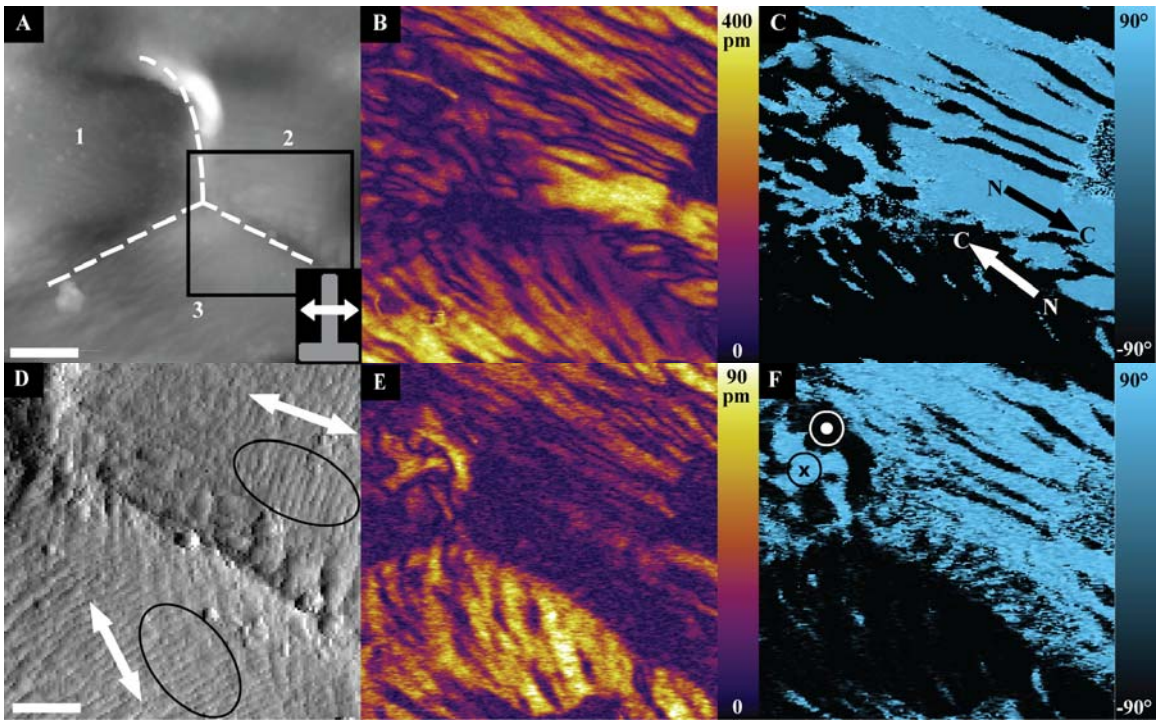

Denning et al Figure 5

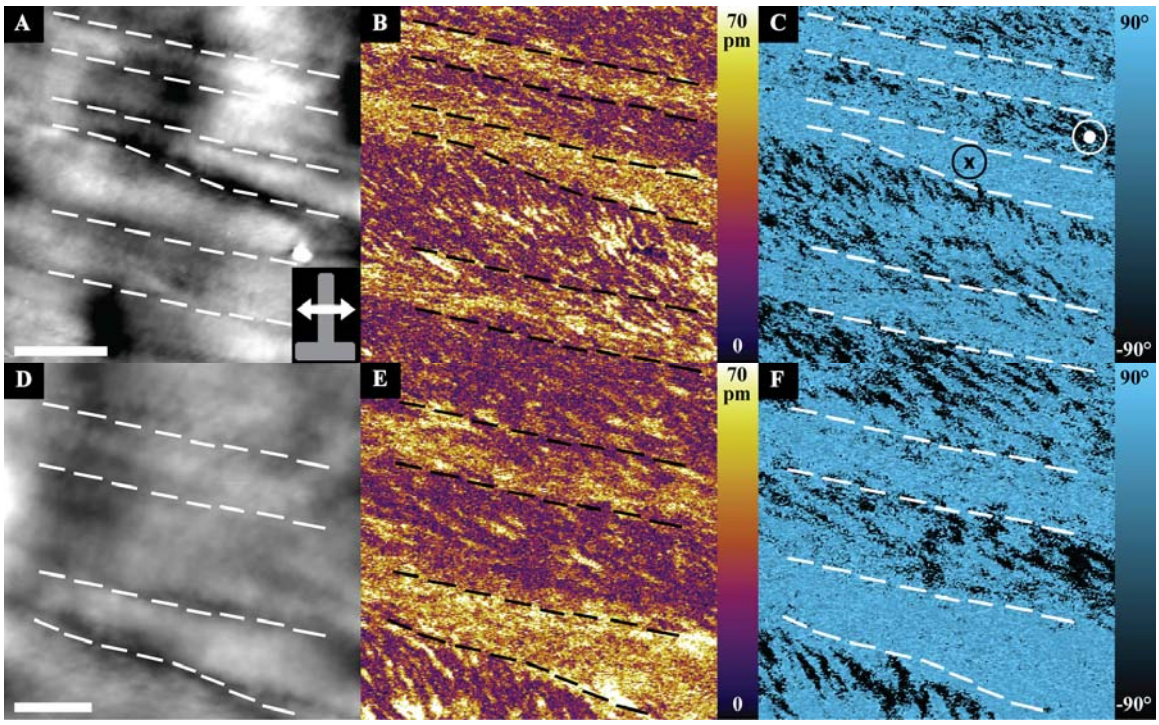

Denning et al Figure 6

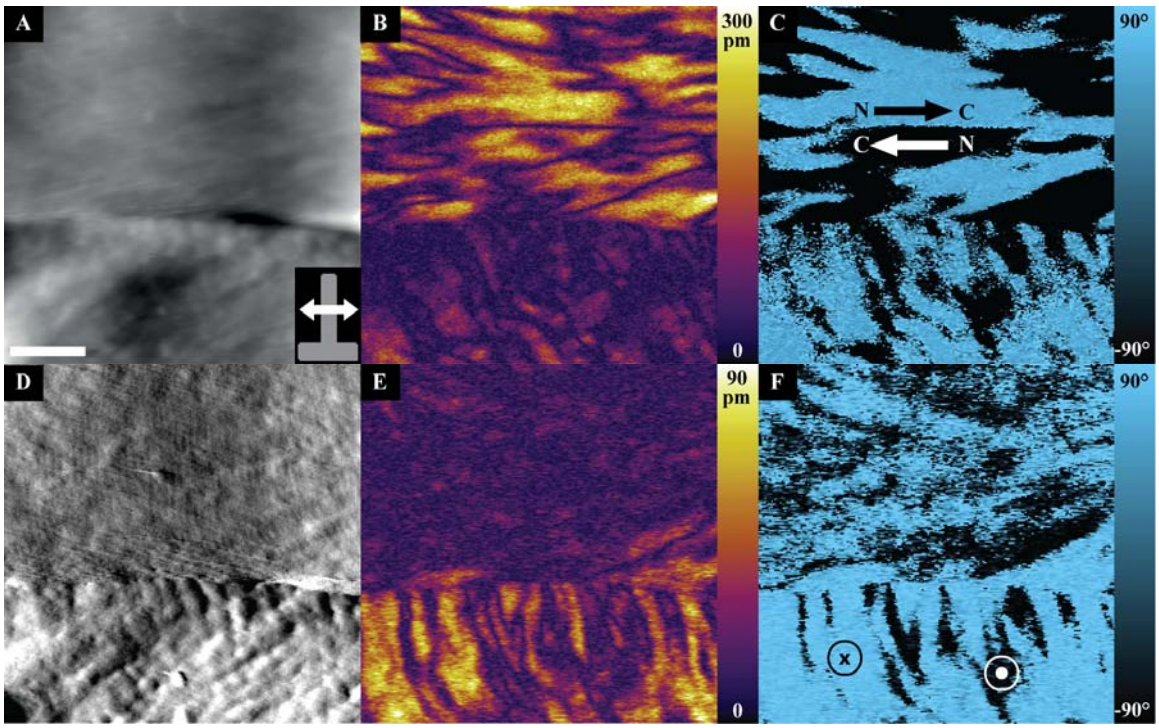

Denning et al Figure 7

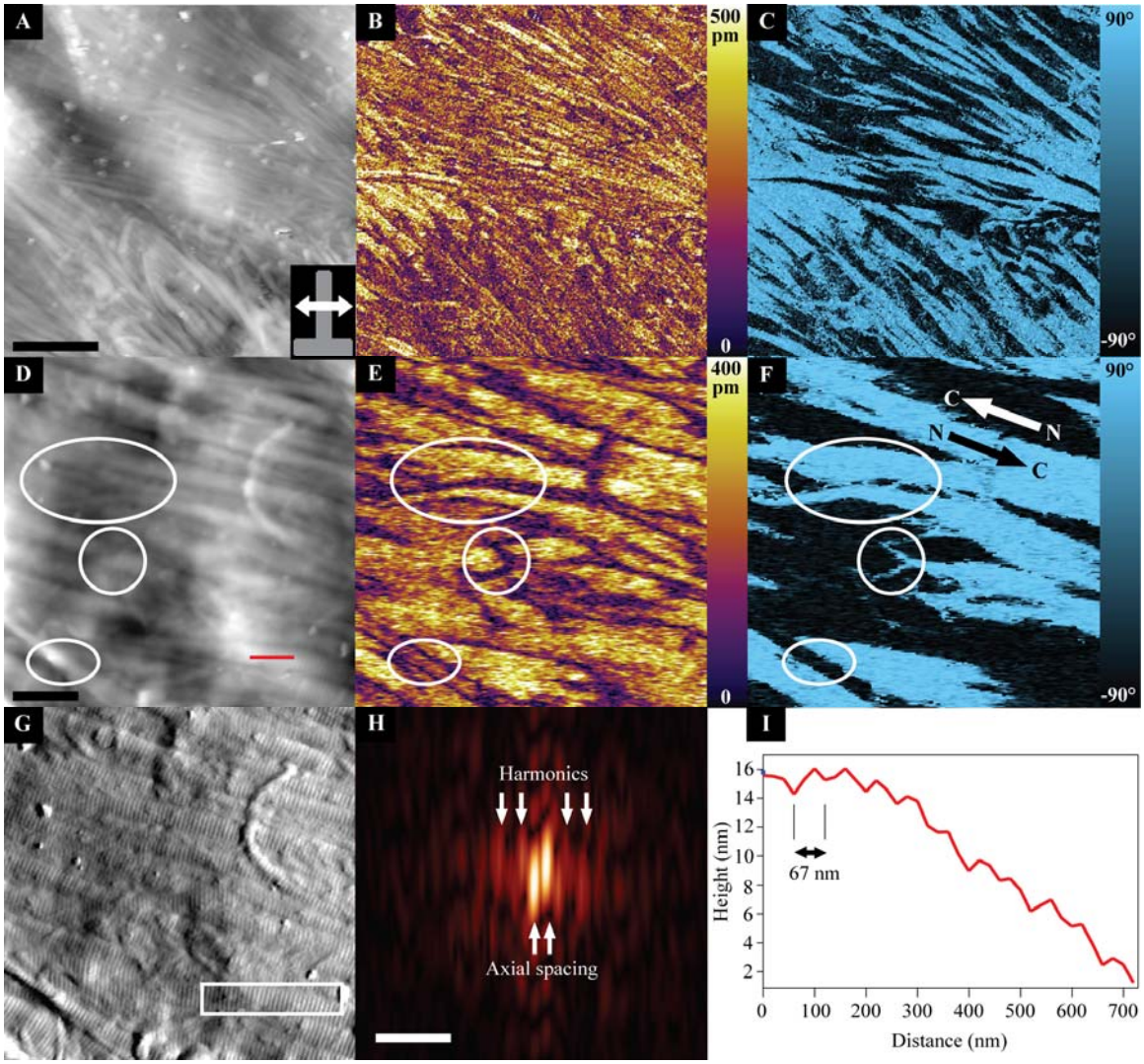

Denning et al Figure 8